JTTEE5 8:414-420

Anisotropic Microstructure of Plasma-Sprayed Deposits

J. Ilavsky, G.G. Long, A.J. Allen, L. Leblanc, M. Prystay, and C. Moreau

(Submitted 23 June 1998; in revised form 3 February 1999)

The microstructure of plasma sprayed deposits (PSD) is dominated by two void systems—interlamellar pores and intralamellar cracks—each with a different anisotropy. Anisotropy of these void systems and varying crack-to-pore ratios within PSDs are responsible for the anisotropic properties observed within deposits. While it is difficult to apply standard porosity measurement techniques to the assessment of anisotropic microstructures, novel techniques utilizing different approaches have recently emerged. Image analysis (IA) of impregnated PSD samples is the most direct technique. The structure is stabilized by impregnation and then polished and imaged. The limitations of IA lie in the impregnation process and in the subsequent polishing. Also, the images produced from anisotropic materials can be difficult to interpret quantitatively. The technique of small-angle neutron scattering (SANS) has recently been applied to the study of PSDs. The major advantages of SANS are that it does not require sample preparation and that quantitative information can be obtained concerning the separate crack and pore systems, including their distinctive anisotropies. However, the relationship between the SANS results and the underlying structure is more complex and less intuitive than for IA, and the availability of the SANS technique is limited by the need to have access to a powerful neutron source, such as a reactor. Also, the two techniques present different views of the microstructure because of the different sensitivities in different parts of the size range. This article compares results from IA and SANS for a set of thick plasma-sprayed ceramic deposits possessing a range of crack/pore microstructures and discusses how the two techniques might complement one another.

Keywords alumina, anisotropy, image analysis, microstructure, small angle neutron scattering, thermally sprayed deposits, yttria-stabilized zirconia

1. Introduction

Plasma spray deposits (PSDs) have a unique, lamellar layered structure (Ref 1), which results in overall anisotropic properties (Ref 2). Optimization of existing and development of new deposits requires an improved understanding of the structure and relationship between the structure and deposit properties.

A number of techniques (Ref 3-5) have been used to study the anisotropic microstructure of these deposits. The most used technique, image analysis (IA), is often applied with sample-preparation and image-enhancing improvements (Ref 6, 7). These improvements are applied to overcome the inherent difficulties of applying this method to studies of thermally sprayed deposits, that is, their fragility and the low imaging contrast of the voids. Impregnation with materials ranging from metals (copper) (Ref 6-9) to epoxy is often necessary (Ref 10). New less damaging grinding and polishing methods are now being used (Ref 11, 12). Image analysis micrographs are processed and evaluated by measuring the angular pore and crack distributions within the sample to determine the presence of anisotropy (Ref 13, 14).

Another technique, developed for PSDs is small angle neutron scattering (SANS). Small-angle neutron scattering can be particularly useful for studying the processing-microstructure relationships of ceramic materials (Ref 15). The total specific surface area of the voids can be derived from the terminal slope in the SANS spectra, that is, Porod scattering (Ref 16). Porod scattering measurements enable a direct determination of the total void specific surface areas in a material independent of the void morphology and regardless of whether the voids are open or closed.

This article compares the anisotropic characterization of the microstructure of plasma sprayed ceramic materials obtained by these two techniques and discusses the similarities and differences in the results.

This paper originally appeared in *Thermal Spray: Meeting the Challenges of the 21st Century; Proceedings of the 15th International Thermal Spray Conference,* C. Coddet, Ed., ASM International, Materials Park, OH, 1998. This proceedings paper has been extensively reviewed according to the editorial policy of the *Journal of Thermal Spray Technology.*

J. Ilavsky, Institute of Plasma Physics, AV CR, Praha, Czech Republic (presently at National Institute of Standards and Technology, U.S. Department of Commerce, 100 Bureau Drive Stop 8523, Gaithersburg, MD, USA); **G.G. Long** and **A.J. Allen,** National Institute of Standards and Technology, Gaithersburg, MD; and **L. Leblanc, M. Prystay,** and **C. Moreau,** National Research Council, Boucherville, Canada. Contact e-mail: ilavsky@ipp.cas.dz.

2. Experimental Techniques

2.1 Small Angle Neutron Scattering

Figure 1 shows a schematic of the SANS experiment. A monochromated and collimated beam of cold neutrons (λ = 0.4 to 2 nm, 0.5 nm in this experiment), with the wavelength deter-

mined by the velocity selector, passes through the sample. These neutrons are scattered within the sample and measured on a two-dimensional detector.

The voids and the grains within the samples have different scattering length density, ρ, causing some of the neutrons to be scattered at the void/grain interfaces. The scattered intensity, *I*, is a function of the scattering wave vector, **Q**, where

$$|\mathbf{Q}| = (4\pi/\lambda)\sin(\theta)$$

and 2θ is the scattering angle (Ref 17). The $I(\mathbf{Q})$ depends on the volume fraction of porosity, ϕ, on the scattering contrast (which is the square of the difference in scattering length densities between the grains and the void, $(\Delta\rho)^2$, and on the distribution of void sizes. When the microstructure of a scattering sample is isotropic, the scattered intensity depends simply on

$$Q = |\mathbf{Q}|$$

rather than on **Q**. (The *Q* represents scalar (value), and the **Q** represents vector.)

The Porod scattering regime (Ref 16,17) extends over the region in the data for which $QL > 3$, where *L* is the smallest dimension in the scatterers. In the absence of anisotropy the scattering cross section, $d\Sigma/d\Omega$, which is proportional to the scattered intensity, is given by the Porod scattering relationship:

$$\frac{d\Sigma(Q)}{d\Omega} = \frac{2\pi(\Delta\rho)^2 S_v}{Q^4} \qquad \text{(Eq 1)}$$

where S_V is the total specific surface area of the voids. Because the material is a two phase (grains + voids) system, where the scattering occurs at the boundaries between solid and void, S_V is the total pore/solid and crack/solid surface area per unit sample volume. To obtain a complete description of the void system, the values for S_V need to be used together with information on the sizes, volumes, and shapes of the voids.

In plasma-sprayed ceramics the voids are preferentially oriented. Here the microstructure is anisotropic, but it is usually circularly symmetric in the substrate plane (Ref 18). To derive the total surface area of voids within an anisotropic material, the scattered intensity can be measured and averaged for all sample-beam orientations, covering all possible angles. For plasma-sprayed samples, this procedure would not necessarily distinguish among the distinct structures in the deposit. Instead, the scattering is measured along selected directions of **Q**, enabling separate derivation of the parameters of the individual void structures that contribute to the anisotropic scattering patterns. The sample is measured in cross section resulting in a two-dimensional distribution of apparent Porod surfaces evaluated from scattering patterns for different orientations of **Q** using Eq 1. Due to the presence of an axis of symmetry perpendicular to the substrate, this two-dimensional distribution can be directly converted into a three-dimensional distribution by rotating the distribution around this axis of symmetry.

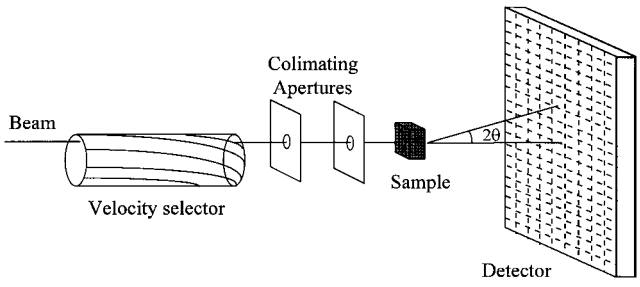

Fig. 1 Schematic for the small angle neutron experiment

The anisotropy in the Porod scattering is strongly amplified by the shape of the scatterers (Ref 19). Even mildly oblate spheroidal scatterers, of fixed orientation, will give markedly prolate anisotropic Porod scattering. Similarly, mildly prolate scatterers, of fixed orientation, will give markedly oblate Porod scattering.

In practice, the anisotropy in the Porod scattering depends not only on the individual pore shapes and preferred orientation, but also on the polydispersity of pore shapes and sizes, and to some extent on the surface roughness. High surface roughness and considerable polydispersity in pore shapes and sizes would produce anisotropic Porod scattering that is linearly proportional to the interfacial surface area projection in the plane perpendicular to **Q** (Ref 16, 17). For random orientations, the anisotropy disappears, and Eq 1 is recovered. However, in the present case of two dominating and coexisting pore/crack morphologies with different preferred orientations and sizes and with relatively smooth interfacial surfaces and geometric symmetries (e.g., oblate spheroidal cracks with parallel sides), two coexisting strong anisotropic distributions may be observable in the three-dimensional distribution of apparent Porod surfaces of plasma-sprayed deposits. Spherical voids, also present in the microstructure (Fig. 2-3) do not contribute significantly to the Porod surface area (because they are large pores with a relatively small surface area) and cannot be distinguished by this technique.

If the Porod scattering can be measured for all orientations of **Q** over a 4π solid angle, a determination of the total interfacial surface area per unit sample volume, $S_{V\,TOTAL}$ is always possible. By averaging $d\Sigma(\mathbf{Q})/d\Omega$ over all orientations of **Q**:

$$\left\langle \frac{d\Sigma}{d\Omega} \right\rangle_{ORIENTATION} = \frac{2\pi|\Delta\rho|^2 S_{V\,TOTAL}}{Q^4} \qquad \text{(Eq 2)}$$

where the <...> brackets imply an orientational average. When different coexisting pore morphologies can be discerned from the orientational variation of $d\Sigma(\mathbf{Q})/d\Omega$, these anisotropic components can be orientationally averaged separately. Thus, $S_{VTOTAL(i)}$ can be determined for the *i*th pore/crack morphology in the system.

2.2 Image Analysis

Image analysis of the cross section of mounted and polished samples is probably the most commonly used technique for microstructural evaluation (Ref 20). However, in the case of plasma sprayed ceramic deposits, it suffers from lack of reproducibility. The main problem with this technique is the sample preparation that involves grinding and polishing. Plasma sprayed ceramic deposits are weak structures, which regularly break and fragment during polishing and, therefore, pullouts are formed. These may significantly obscure the structure (Ref 21).

Various improvements were proposed for the preparation of polished surfaces of these weak structures. Infiltration of pores with epoxy combined with careful polishing and cautious evalu-

ation of images offers a most valuable insight into the shapes of the voids and orientations (Ref 13).

In the present experiment, samples were infiltrated with epoxy, cut with a diamond saw through their thickness, remounted in epoxy and carefully polished using SiC papers and diamond slurries. As mentioned previously, the polishing method is very important in imaging these structures. Impregnation with epoxy significantly reduces damage in the forms of pullouts, which are extensively formed using standard preparation and polishing techniques. Progress of polishing was checked regularly by optical microscopy. Each sample required different times at each polishing step, depending on its resistance to form pullouts.

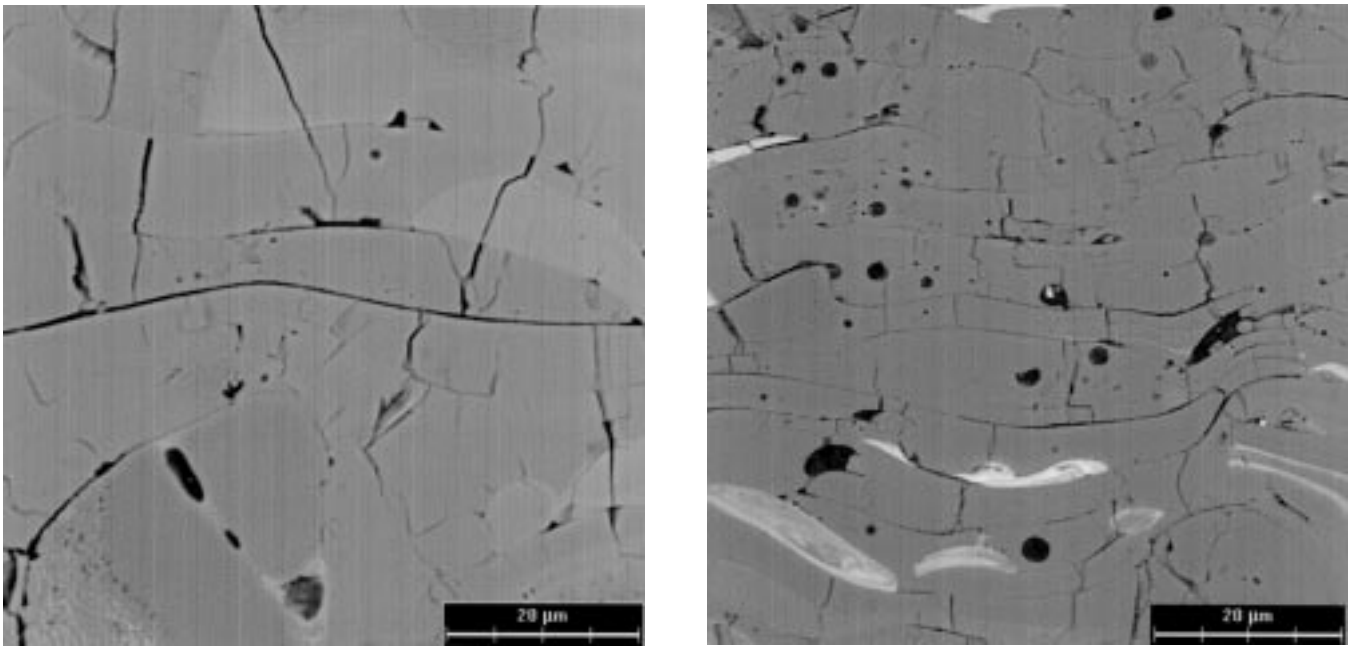

(a) (b)

Fig. 2 Micrographs of (a) water-stabilized plasma alumina and (b) gas-stabilized plasma alumina. The scanning electron microscopy mode was back scattered electrons. 1500×

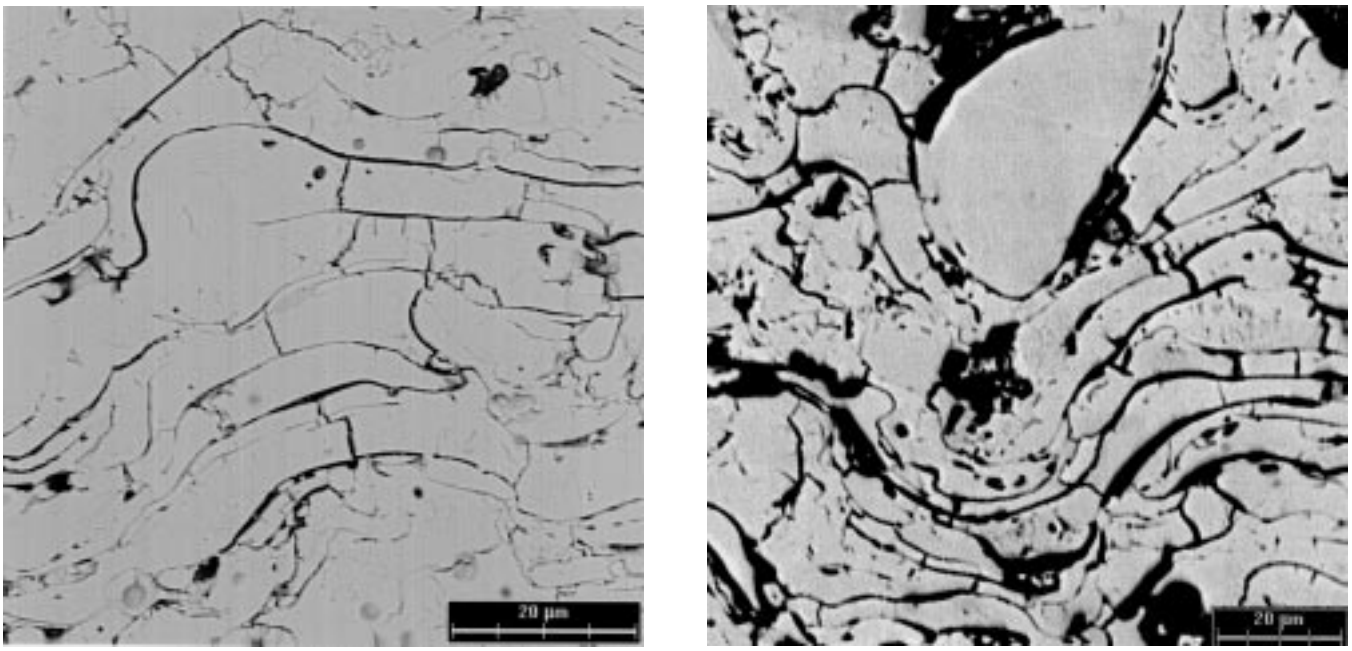

(a) (b)

Fig. 3 Micrographs of (a) as-sprayed gas-stabilized plasma yttria-stabilized zirconia (Amdry sample) and (b) annealed gas-stabilized plasma yttria-stabilized zirconia (Amdry sample). The scanning electron microscopy mode was back scattered electrons. 1500×

Therefore, it is not practical to specify a single procedure for all of these samples.

Polished cross sections of selected samples were studied using scanning electron microscopy. Five digital images acquired at 500× magnification from a single cut of each sample were stored to disk. Using such a low magnification allows a characterization of the sample crack distribution with a reasonable number of images. However, small and/or narrow cracks can be difficult to resolve.

Image analysis was performed on each image to measure the sample angular crack distribution. A summary of the algorithm applied is:

- Threshold the image. Using the binary image, voids (pores and cracks) are skeletonized until they are one pixel wide.
- All intersecting cracks are broken at the intersection. This gives the net effect of having several single cracks lying in specific directions rather than one large crack network.
- The length, major and minor axes, and the angular orientation of each crack is measured.

Note that this process measures the two-dimensional projection of the three-dimensional orientational distribution of the voids system. The end result of this algorithm is to treat each pore or crack as an individual feature of equal weighting. Therefore, no results regarding their volume or surface area can be deduced.

3. Experiment

A water-stabilized plasma (WSP) spray system (PAL160, Institute of Plasma Physics, Academy of Sciences of the Czech Republic, Prague, Czech Republic) and a gas-stabilized plasma (GSP) spray system (F4, Plasma Technik, A.G., Germany) were used to prepare the samples. The WSP system was operated at approximately 160 kW input (320 V, 500 A) with about 35 kg/h (approximately 583 g/min) of alumina feedstock fed through two injectors. The feeding distance (distance between the torch nozzle to external powder injector) was 30 mm, and the spray distance (distance between the torch nozzle and substrate) was 350 mm. The spray nozzle diameter was 8 mm for the GSP system, the powder injector diameter was 1.8 mm, and the current was 500 A at 68 V. The primary gas was argon (40 slpm, or L/min), the secondary gas was hydrogen (10 slpm, or L/min), and the carrier gas was argon (3 slpm, or L/min). The powder feed rate was about 1.5 kg/h (26 g/min). The spray distance was 90 mm for Amdry feedstock (Amdry 142, from Sulzer Plasma Technik Inc., Troy, MI) and 145 mm for SX feedstock (SX233, Osram Sylvania Inc., Danvers, MA). Table 1 lists the parameters for the feedstock.

To obtain free-standing deposits, approximately 5 mm thick deposits were sprayed onto a mild steel substrate (50 by 25 by 2.5 mm) that had previously been covered with an aluminum layer (deposited by wire-arc spraying). After spraying, the aluminum layer was dissolved in HCl to obtain free-standing deposits. A low speed diamond saw was used for sectioning the samples.

Both ZrO_2 + 8% Y_2O_3 yttria-stabilized zirconia (YSZ) samples (made from Amdry and SX233 feedstock) were studied as-sprayed and annealed in air at 1100 °C for 1 h. The heating and cooling rate of the furnace was 600 °C/h, with the cooling rate being lower at temperatures below approximately 800 °C.

4. Results

Results of the SEM imaging are presented in Fig. 2 and 3. Figures 4 to 6 graphically present the SANS results. An explanation of void systems surface area separation is graphically presented in Fig. 7. Table 2 gives the numerical results. Results of IA of alumina samples are shown in Fig. 8 and those of zirconia samples in Fig. 9.

Table 1 Parameters of the feedstock materials

Manufacturer/ material	Composition, mass fraction, %	Size range(a), d_{10}, d_{90}, μm	Spray method(b)
Alloy Metals/Amdry 142	ZrO_2, 8%Y_2O_3	41, 113	GSP
Sylvania/SX233	ZrO_2, 8%Y_2O_3	26, 96	GSP
Norton/gray alumina	Al_2O_3 + 2.7% TiO_2, 0.8% SiO_2, 0.1 % Fe_2O_3, and 0.6% other oxides	46, 124	WSP
Metco/101B-NS	Al_2O_3 + 2.5% TiO_2, 2% SiO_2, 1% Fe_2O_3 and 0.5% of other oxides	40, 116	GSP

(a) 10% of the diameters were smaller than d_{10}, and 90% of the diameters were smaller than d_{90}. (b) GSP, gas-stabilized plasma spraying, WSP, water-stabilized plasma spraying

Table 2 Results of the small-angle neutron scattering analysis

	Material and cracks/pores ratio(a), total voids surface area			
Spray process	WSP alumina	GSP alumina	Amdry YSZ	SX YSZ
As-sprayed	85:15 1.73 10^4cm^2/cm^3	50:50 1.47 10^4cm^2/cm^3	15:85 2.78 10^4cm^2/cm^3	NA 1.49 10^4cm^2/cm^3
Annealed 1 h at 1100 °C	NA	NA	0:100 1.84 10^4cm^2/cm^3	0:100 1.29 10^4cm^2/cm^3

Estimated errors for fractions are ±5, for specific surface areas ±0.05 10^4cm^2/cm^3. *XX*:*YY* represents fractions of surface areas in cracks:(interlamellar) pores.

5. Discussion

The micrographs of Fig. 2(a) and (b) and Fig. 3(a) and (b) show the complexity of the PSD microstructures. These microstructures are composed of two anisotropic void systems, interlamellar pores and intralamellar cracks, and a range of nearly spherical voids. Micrographs indicate that the intralamellar crack network extends over a wide range of sizes and that there are large, micrometer-sized cracks crossing whole splats as well as fine, much smaller cracks within the splats. These fine cracks within the splats, best visible in (Fig. 3a), are probably inaccessible to an impregnating medium (epoxy, copper, etc.) and also difficult to recognize under lower magnifications.

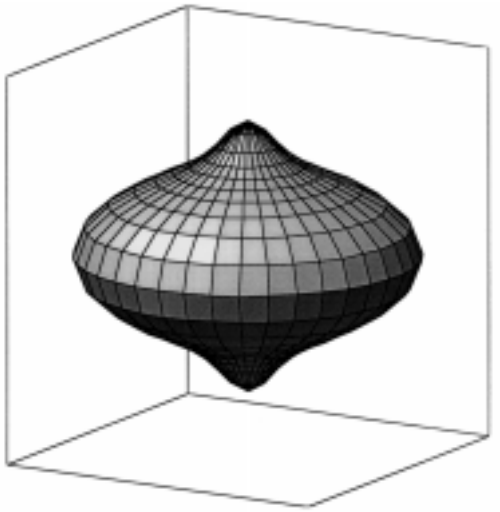

Fig. 4 Apparent Porod surface area distribution of water-stabilized plasma deposited alumina. Apparent Porod surface area can be defined as the Porod surface area, which would be viewed in any particular direction by an observer standing in the center of the sample. Knowledge of this apparent surface area in all directions (over 4π) allows calculation of the quantitative specific surface area in the sample and, if more surface systems can be distinguished, in the surface systems separately.

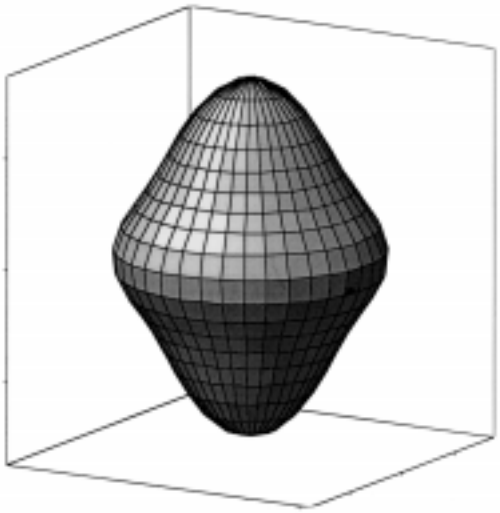

Fig. 5 Apparent Porod surface area distribution of gas-stabilized plasma deposited alumina. For explanation of apparent Porod surface area see caption of Fig. 4.

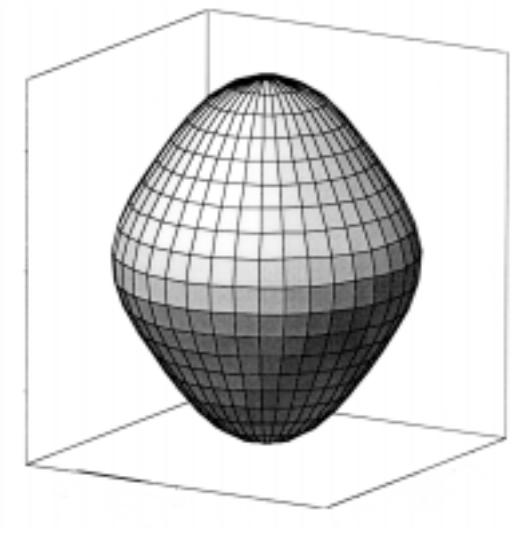

(a)

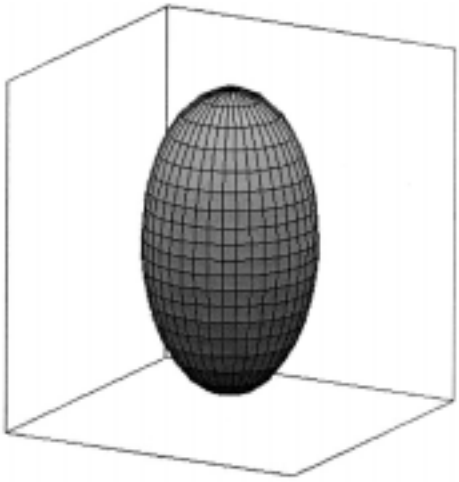

(b)

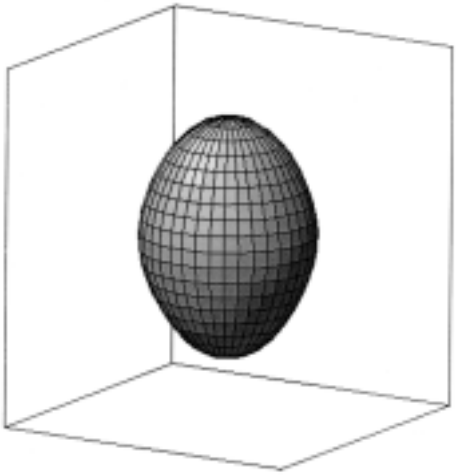

(c)

Fig. 6 Apparent Porod surface area distribution of gas-stabilized plasma deposited zirconia. For explanation of apparent Porod surface area see caption of Fig. 4. Amdry (a) as sprayed, (b) annealed, and (c) SX as sprayed. The figure for annealed SX sample was very similar to the figure for annealed Amdry sample and is therefore not presented.

The resolution limit of the SANS technique is around 3 nm void diameter. However, if such sized voids would be present, they would be observable in the SANS spectra. The SANS regime used allows estimation of a minimum void size larger than 20 nm in diameter.

The IA technique used in this work used a magnification of 500×, whereas Fig. 2 and 3 used a magnification of 1500×. Using lower magnification allowed sufficient data to be obtained for a good statistical analysis with a reasonable number (five) of micrographs. However, the resolution limit was larger, and it can be expected, therefore, that fine voids may have been neglected.

This fact can be illustrated by comparing results from SANS (Fig. 4 and 5) and IA (Fig. 8). Water stabilized plasma alumina SANS results in Fig. 4 show high anisotropy of the apparent Porod surface area distribution dominated by intralamellar cracks; whereas the same sample gave a lower anisotropy in the IA results (Fig. 8) than GSP alumina. Note in Fig. 7 how this apparent Porod surface area distribution relates to the two observable void systems—interlamellar pores and intralamellar crack. The GSP alumina SANS results were more balanced—both void systems had about the same surface area, Table 2, and the apparent surface area anisotropy was clearly different (Fig. 5). However, the IA results of the GSP alumina (Fig. 8) showed higher anisotropy than WSP alumina and were dominated by interlamellar pores. A likely explanation is that IA is missing a large number of intralamellar cracks due to their small size.

Even more persuasive are results obtained on the YSZ samples. Both as-sprayed YSZ samples were dominated on SANS and in IA by interlamellar pores (Fig. 6 and 9).The SANS results in Fig. 6(a) and (c) show that the as-sprayed Amdry deposit was more anisotropic than the SX deposit, which is confirmed by the IA result in Fig. 9. Here both techniques seem to agree.

However, the same Fig. 6 shows, as well as Table 2, that annealing of YSZ resulted in a significant increase of the void anisotropy. Figure 7 shows how the anisotropy of the apparent Porod surface area distribution can be used to separate the two dominating void systems. Results in Table 2 show that the anisotropy increases after annealing due to the sintering away of intralamellar cracks so that their surface area decreases beyond the resolution limit of this technique. Such a change in the anisotropy was not observed in the IA results. Note that because the large voids (e.g., large intralamellar cracks) have relatively low surface area they may not be detectable in the SANS results even though they may be observable by IA. The disappearance of fine intralamellar cracks can be observed only with difficulty on large magnification micrographs (Fig. 3). In this case the IA technique did not resolve some artifacts of the microstructure.

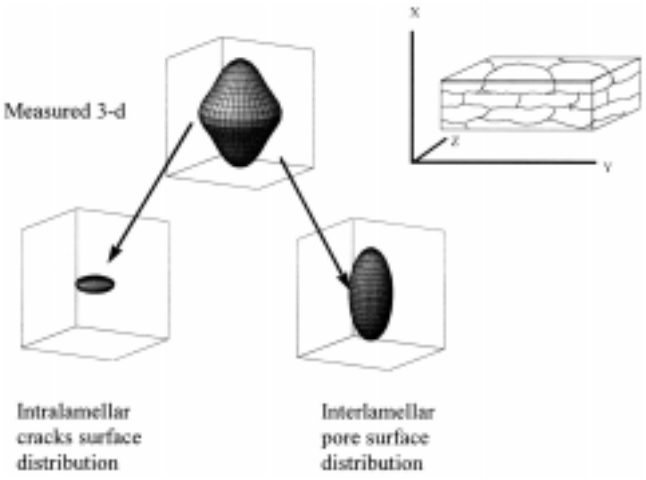

Fig. 7 The apparent Porod surface area distribution of gas-stabilized plasma deposited alumina separated into two separate void surface areas. Left (prolated ellipsoid) representing intralamellar cracks and right (elongated ellipsoid) representing interlamellar pores. For explanation of apparent Porod surface area see caption of Fig. 4. Axes descriptions, labels and tick marks are the same as for Fig. 4 and are left out for clarity purposes. Orientation of axes with respect to the deposit is also depicted.

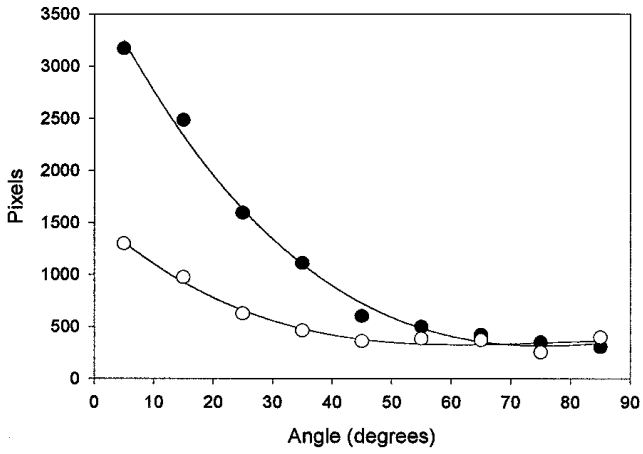

Fig. 8 Angular voids distribution determined by image analysis in alumina deposits sprayed with different techniques. Gas-stabilized plasma sprayed alumina, closed circles (●), and water-stabilized plasma alumina, open circles (○). Voids parallel to the surface (i.e., interlamellar pores) are at 0°, while voids perpendicular to the surface (i.e., intralemellar cracks) are at 90°. Estimated standard uncertainties are ±7%.

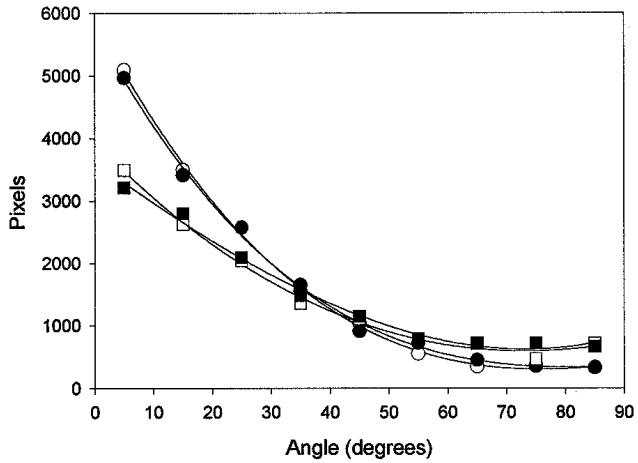

Fig. 9 Angular voids distribution determined by image analysis for yttria-stabilized zirconia deposits. Amdry samples (circles) and SX samples (squares). Open symbols correspond to as-sprayed deposits whereas closed symbols correspond to heat treated samples. Voids parallel to the surface (i.e., interlamellar pores) are at 0° while voids perpendicular to the surface (i.e., intralamellar cracks) are at 90°. Estimated standard uncertainties are ±7%.

The importance of these fine cracks is underlined by a significant (50 to 100%) increase in Young's modulus after similar annealing reported in Ref 22.

6. Conclusions

The following conclusions can be drawn*:

The anisotropy of the plasma sprayed deposits can be studied by various methods. It is important to understand the limitations of each method and to consider them for any given application. Image analysis can be a very successful technique when there is interest in large features within the microstructure or in major differences between the deposits. The SANS technique has a much finer size resolution limit and produces more complete, quantitative, and often separate results on void structures. However, in its present form it has difficulty including features such as the larger spherical voids observed in micrographs. More studies applying both these techniques may be needed to obtain a complete view of the complex microstructure of sprayed deposits.

Acknowledgment

Partial support of J. Ilavsky by a grant of the Czech Grant agency (GACR 202/98/P06) is gratefully acknowledged.

References

1. H. Herman, Plasma-Sprayed Coatings, *Sci. Am.*, Vol 259 (No. 3), 1988, p 112-117
2. H. Nakahira, K. Tani, K. Miyajima, and Y. Harada, Anisotropy of Thermally Sprayed Coatings, *Thermal Spray: International Advances in Coatings Technology*, C.C. Berndt, Ed., ASM International, 1992, p 1011-1017
3. H.E. Exner and M. Fripan, Quantitative Assessment of Three-Dimensional Roughness, Anisotropy and Angular Distributions of Fracture Surfaces by Stereometry, *J. Microsc.*, Vol 138 (No. 2), 1985, p 161-178
4. S.H. Leigh, G. Montavon, C. Coddet, S. Sampath, H. Herman, and C.C. Berndt, Quantitative Analysis of Thermal Spray Deposits Using Stereology, *Advances in Thermal Spray Science and Technology*, C.C. Berndt and S. Sampath, Ed., ASM International, 1995, p 273-278
5. G. Montavon, S.H. Leigh, S. Sampath, H. Herman, C.C. Berndt, and C. Coddet, Stereological Analysis of Thermally Sprayed Deposits, *Advances in Thermal Spray Science and Technology*, C.C. Berndt and S. Sampath, Ed., ASM International, 1995, p 279-283
6. K.A. Leithner, Basics of Quantitative Image Analysis, *Adv. Mater. Process.*, Vol 11, 1993, p 18-23
7. G. Montavon, C. Coddet, C.C. Berndt, and S.H. Leigh, Microstructural Index to Quantify Thermal Spray Deposit Microstructures Using Image Analysis, *J. Therm. Spray Technol.*, Vol 7 (No. 2), 1998, p 229-241
8. C.-J. Li, A. Ohmori, and Y. Arata, Effect of Spray Methods on the Lamellar Structure of Al_2O_3 Coatings, *Thermal Spraying—Current Status and Future Trends*, A. Ohmori, Ed., High Temp. Soc. of Japan, Ibaraki, Osaka, Japan, 1995, p 501-506
9. S. Boire-Lavigne, C. Moreau, and R.G. Saint-Jacques, The Relationship between the Microstructure and Thermal Diffusivity of Plasma-Sprayed Tungsten Coatings, *J. Therm. Spray Technol.*, Vol 4 (No. 3), 1995, p 261-267
10. J. Karthikeyan, Vacuum Impregnation of Sprayed Coatings for Microstructural Studies, *Thermal Spraying—Current Status and Future Trends*, A. Ohmori, Ed., High Temp. Society of Japan, Ibaraki, Osaka, Japan, 1995, p 927-932
11. S.D. Glancy, Pursuit of a Universal Metallographic Procedure for Thermally Sprayed Coatings, *1995 Advances in Thermal Spray Science and Technology*, C.C. Berndt and S. Sampath, Ed., ASM International, 1995, p 493-498
12. S.H. Leigh, Stereological Investigation on Structure/Property Relationships of Plasma Spray Deposits, Ph.D. thesis, State University of New York at Stony Brook, May 1996
13. S. Boire-Lavigne, C. Moreau, and R.G. St. Jacques, Taguchi Analysis of the Influence of Plasma Spray Parameters on the Microstructure of Tungsten Coatings, Developments, and Applications of Ceramics and New Metal Alloys, *Proceedings of International Symposium on Developments and Applications of New Ceramics and Metals Alloys* (Quebec, Canada), R.A.L. Drew and H. Mostaghaci, Ed., 29 Aug to 2 Sept 1993, p 473-485
14. M. Prystay, P. Gougeon, and C. Moreau, Correlation between Particle Temperature and Velocity and the Structure of Plasma Sprayed Zirconia Coatings, *Thermal Spray: Practical Solutions for Engineering Problems*, C.C. Berndt, Ed., ASM International, 1996, p 517-523
15. J. Ilavsky, A.J. Allen, G.G. Long, S. Krueger, C.C. Berndt, and H. Herman, Influence of the Spray Angle on the Pore and Crack Microstructure of Plasma Sprayed Deposits, *J. Am. Ceram. Soc.*, Vol 80 (No. 3), 1997, p 733-742
16. G. Porod, *Small-Angle X-Ray Scattering*, O. Galtter and O. Kratky, Ed., Academy Press, London, 1982, p 17
17. G. Kostorz, Small-Angle Scattering and Its Applications to Materials Science, *Treatise on Materials Science and Technology*, Vol 15, G. Kostorz, Ed., Academic Press, 1979, p 227
18. J. Ilavsky, H. Herman, C.C. Berndt, A.N. Goland, G.G. Long, S. Krueger, and A.J. Allen, Porosity in Plasma Sprayed Alumina Coatings, *1994 Thermal Spray Industrial Applications*, C.C. Berndt and S. Sampath, Ed., ASM International, 1994, p 709-714
19. F.M. Hamzeh and R.H. Bragg, Small-Angle Scattering of X-Rays from Groups of Nonrandomly Oriented Ellipsoids of Revolution of Low Concentration, *J. Appl. Phys.*, Vol 45 (No. 7), 1974, p 3189-3195
20. D.B. Fowler, W. Riggs, and J.C. Russ, Image Analysis Applied to Thermal Barrier Coatings, *Thermal Spray Research and Applications*, T.F. Bernecki, Ed., ASM International, 1990, p 303-313
21. J.P. Sauer, Metallographic Preparation of Thermal Spray Coatings: Coating Sensitivity and the Effect of Polishing Intangibles, *Thermal Spray: Practical Solutions for Engineering Problems*, C.C. Berndt, Ed., ASM International, 1996, p 777-783
22. J.S. Wallace and J. Ilavsky, Elastic Modulus Measurements in Plasma Sprayed Deposits, *Thermal Spray: A United Forum for Scientific and Technological Advances*, C.C. Berndt, ASM International, 1997, p 757-762

*Note: Certain commercial materials are identified in order to adequately specify the experimental procedure. Such identification does not imply recommendation or endorsement by the National Institute of Standards and Technology, nor does it imply that it is necessarily the best available for the purpose.